

Original paper

Línkite, $K_2Ca_3[(UO_2)(CO_3)_3]_2 \cdot 8H_2O$, a new uranyl carbonate mineral from Jáchymov, Czech Republic

Jakub PLÁŠIL^{1*}, Jiří ČEJKA², Jiří SEJKORA², Jan HLOUŠEK[†], Radek ŠKODA³, Milan NOVÁK³, Michal DUŠEK¹, Ivana ČISAŘOVÁ⁴, Ivan NĚMEC⁴, Jana EDEROVÁ⁵

¹ Institute of Physics, Academy of Sciences of the Czech Republic v.v.i, Na Slovance 2, 182 21 Prague 8, Czech Republic; plasil@fzu.cz

² Department of Mineralogy and Petrology, National Museum, Cirkusová 1740, 193 00 Prague 9, Czech Republic

[†] Jáchymov; deceased on April 27, 2014

³ Department of Geological Sciences, Faculty of Science, Masaryk University, Kotlářská 2, 611 37 Brno, Czech Republic

⁴ Department of Inorganic Chemistry, Faculty of Science, Charles University, Hlavova 8, 128 43 Prague 2, Czech Republic

⁵ Institute of Chemical Technology, Technická 5, 166 28 Prague 6, Czech Republic

* Corresponding author



Línkite, $K_2Ca_3[(UO_2)(CO_3)_3]_2 \cdot 8H_2O$, is a new uranyl tricarbonate mineral from Jáchymov, Western Bohemia, Czech Republic. It occurs in association with grimselite, andersonite, liebigite, čejkaite, schröckingerite, agricolaite, ježekite and braunerite. Línkite forms from uranium-rich aqueous solutions and its origin is associated with post-mining processes. Línkite is orthorhombic, space group $Pnmm$, with $a = 17.0069(5)$ Å, $b = 18.0273(5)$ Å, $c = 18.3374(5)$ Å and $V = 5622.1(2)$ Å³, and $Z = 8$. It forms tabular, mostly isometric crystals, up to $c.$ 0.5 mm across, typically in multiple intergrowths. The color is pale olive to khaki green and it has a greenish white to yellowish white streak. Crystals are transparent and have vitreous luster. The Mohs hardness is estimated to be between 2 and 3. Línkite is brittle with an uneven fracture and perfect cleavage on $\{100\}$ and very good cleavage on $\{010\}$. It exhibits intense greenish yellow luminescence under both short- (254 nm) and long-wave (366 nm) UV radiation. The calculated density is 2.922 g/cm³. The mineral is biaxial (+) with indices of refraction, $\alpha = 1.546(2)$, $\beta = 1.550$, $\gamma = 1.562(2)$. The $2V_{obs}$ is moderate; the calculated $2V$ is +60°. Optical orientation: $Y = a, X = b, Z = c$. The electron microprobe analyses (average of 28) provided: Na₂O 0.06, K₂O 6.89, CaO 14.11, CuO 0.12, UO₃ 48.76, CO₂* 22.51, H₂O* 12.20 (~12.9 from TG) (*calculated), total 104.65 wt%. The empirical formula (based on 30.22 O apfu) is: $(K_{1.73}Na_{0.02})_{\Sigma 1.75}(Ca_{2.97}Cu_{0.02})_{\Sigma 2.99}[(UO_2)(CO_3)_3]_{2.02}(H_2O)_{8.00}$. The Raman and infrared spectra exhibit prominent features consistent with the mineral being a hydrated uranyl tricarbonate, with fundamental vibrations of H₂O molecules, CO₃²⁻ anions and UO₂²⁺ ions. The seven strongest powder X-ray diffraction lines are [d_{obs} in Å (hkl) I_{rel}]: 8.627 (200) 100, 6.436 (022) 60, 5.935 (212) 11, 5.153 (222) 43, 4.592 (004) 19, 4.505 (040) 12 and 4.053 (204) 15. The structure of línkite was refined from single-crystal X-ray data to $R = 0.034$ for 4468 unique observed reflections ($I_{obs} > 3\sigma I$). The structure consists of prominent $(Ca(H_2O)_2[(UO_2)(CO_3)_3])^{2-}$ layers parallel to (100), which define a square grid, leading to a strong tetragonal pseudosymmetry of línkite. Between the layers, disordered K⁺ cations and H₂O molecules are localized. The structure is closely related to other uranyl tricarbonate minerals, e.g., albrechtschraufite and andersonite, due to the presence of a very characteristic paddle-wheel motif, $Ca[(UO_2)(CO_3)_3]_4Ca$.

Keywords: Línkite, uranyl carbonate, crystal structure, Raman spectroscopy, Jáchymov

Received: 11 June 2017; accepted: 21 August 2017; handling editor: F. Laufek

The online version of this article (doi: 10.3190/jgeosci.241) contains supplementary electronic material.

1. Introduction

Uranyl carbonate minerals are thermodynamically favored to precipitate from neutral- to alkaline aqueous solutions containing dissolved CO₃²⁻ ions (Langmuir 1978). The activity of carbonate species is usually maintained by the dissolution of gangue carbonates, which are commonly associated with primary uraninite on most hydrothermal veins. Until recently the twenty-six uranyl carbonates have been described as minerals (Krivovichev and Plášil 2013). The Jáchymov ore district is famous namely for the occurrences of uranyl minerals, and among them uranyl carbonates have been of particular interest in the

past, as it is well documented e.g. by the early description of the uranyl carbonate–sulfate mineral schröckingerite, already in 1873 (Schrauf 1873; Mereiter 1986a). Several remarkable uranyl carbonate minerals were described from Jáchymov as their type locality; among them albrechtschraufite, $MgCa_4F_2[(UO_2)(CO_3)_3]_2(H_2O)_{17-18}$ (Mereiter 1984; 2013), čejkaite, $Na_4[(UO_2)(CO_3)_3]$ (Ondruš et al. 2003; Plášil et al. 2013) and agricolaite, $K_4[(UO_2)(CO_3)_3]$ (Skála et al. 2011). In this paper we provide the description of a new uranyl tricarbonate mineral from Jáchymov, línkite, ideally $K_2Ca_3[(UO_2)(CO_3)_3]_2 \cdot 8H_2O$, Strunz Class 05.ED, which is the first member containing alkalis to alkaline earths in the ratio 2:3.

Línkite is named in honor of Dr. Allan Líněk (1925–1984), a Czech physicist and crystallographer of the Institute of Physics, Academy of Sciences of the Czech Republic, for his significant contribution to structure science.

The new mineral and its name have been approved by the Commission on New Minerals, Nomenclature and Classification (CNMNC) of the International Mineralogical Association (IMA 2012–066). The description of the mineral is based upon material from the holotype specimen, which is now deposited in the collections of the Department of Mineralogy and Petrology of the National Museum in Prague, Cirkusová 1740, Prague 9, Czech Republic, catalog number P1P 2/2012.

2. Sample

Línkite was discovered in an old mine adit on the Geschieber vein, at the 5th level of the Svornost (Einigkeit) mine, Jáchymov ore district, Western Bohemia, Czech Republic. The mineral was found by one of the authors (JH) on the muddy or dusty surfaces of the surrounding country rocks (dominantly dark amphibole schist) and, less commonly, also in gangue material lying as gravel on the footwall of the crossing-adit leading to the vein. Liebigite, grimselite, andersonite, čejkaite, schröckingerite, agricolaite, ježekite (Plášil et al. 2015), braunerite (IMA 2015–123, Plášil et al. 2016), and gypsum occur closely associated with línkite.

Since no primary uranium mineral or its relics were found on the specimens, we conclude that the mineral assemblage of uranyl carbonates and sulfates formed from U-rich solutions, most probably containing uranyl-carbonate complexes that migrated from the primary

sites. These solutions were likely alkaline or neutral. The presence of $(\text{SO}_4)^{2-}$ anions (in schröckingerite and in ježekite) is due to abundance of pyrite in the associated black schist. The mineral assemblage in which línkite occurs is typical of recent/subrecent association related to post-mining processes.

3. Physical and optical properties

Línkite occurs as well-formed thin tabular crystals, up to 0.5 mm in size, forming aggregates of sub-parallel intergrown crystals (Fig. 1). Their aggregates reach up to 1.2 mm across. Línkite crystals show a dominant {100} pinacoid form, and prism forms {101}, {110} and {011} (Fig. 2). The color is pale olive to khaki green. The streak is greenish white to yellowish white and luster is vitreous. Línkite exhibits intense greenish yellow luminescence under both short- (254 nm) and long-wave (366 nm) UV radiation. The Mohs hardness ranges between 2 and 3. The new mineral is brittle with uneven fracture and a perfect cleavage on {100} and a very good cleavage on {010}. The calculated density based on the empirical formula is 2.922 g/cm³. The mineral is optically biaxial (+) with the following indices of refraction, measured using 589 nm light: $\alpha = 1.546(2)$, $\beta = 1.550$, $\gamma = 1.562(2)$. The index β was measured only once due to the lack of appropriately oriented crystal fragments. $2V_{\text{obs}}$ is moderate but the exact value could not be measured as the conoscopic figures were of a low quality; calculated $2V$ is $+60^\circ$. Optical orientation: $Y = \mathbf{a}$, $X = \mathbf{b}$, $Z = \mathbf{c}$. Línkite is pale khaki green and non-pleochroic in transmitted light. It dissolves quickly in 10% HCl with the release of CO₂ observed as bubbles.



4. Thermal analysis

A thermogravimetric study of línkite (Fig. 3) was performed on a Stanton Redcroft Thermobalance TG 750 in the range 20–900 °C, with a heating rate of 10 °C/min, in a dynamic air atmosphere, a flow rate of 10 ml/min and a sample weight of 1.422 mg.

Thermal experiment documented that línkite dehydrates in three distinct steps (Fig. 3;

Fig. 1 The aggregate of tabular línkite crystals growing on the rock fragment. Width of photograph 2 mm, photo by Pavel Škácha.

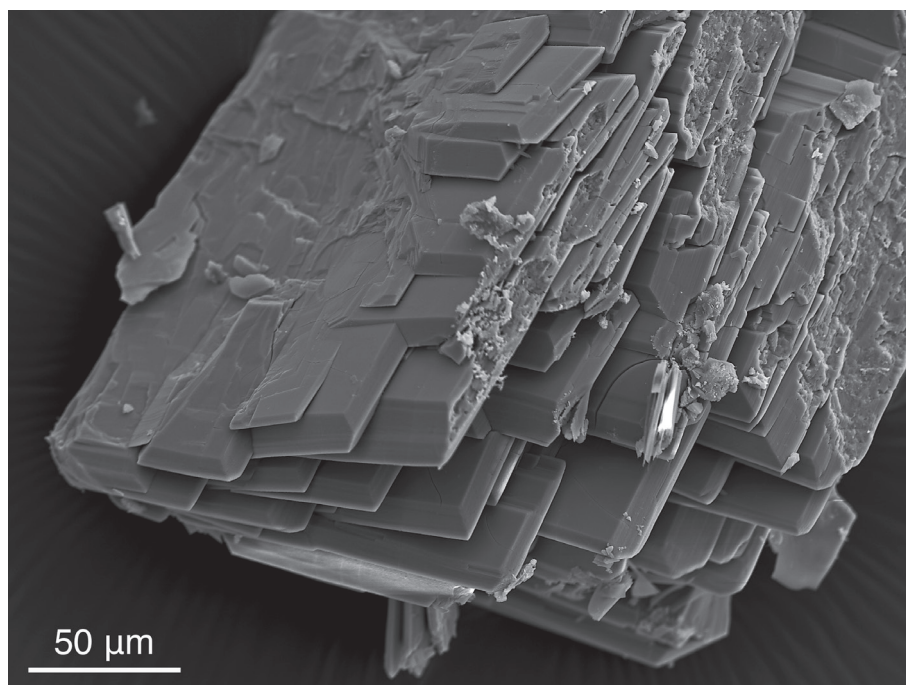


Fig. 2 The aggregate of linekrite tabular crystals. Secondary-electron image (Jeol JSM-6370).

Tab. 1). Schematically, the whole process up to 413 °C can be described as the release of 5 H₂O (up to 125 °C), 2 H₂O (between 125 and 188 °C), and 1 H₂O and 1 CO₂ (up to 413 °C) (Tab. 1). Some overlap of processes, dehydration and decarbonation, is possible. Additional CO₂ molecules (3 CO₂ and 2 CO₂) are released up to 900 °C. The full dehydration and carbon dioxide release are connected with the destruction of the linekrite crystal structure. The end-product of the thermal decomposition of linekrite is most probably (K,Ca)-uranate similar to the case of thermal decomposition of andersonite, when (Na,Ca)-uranate is formed (Čejka 1969). The total content of molecular water in linekrite inferred from the thermal analysis is ~8 H₂O (Tab. 1).

5. Chemical composition

Electron microprobe analyses (28 representative points) were performed at the Masaryk University in Brno using a Cameca SX-100 electron microprobe (WDS mode, 15 kV, 2 nA, 15 μm beam diameter). The following X-ray lines and standards were selected to minimize line overlaps; *K_α* lines: Ca (grossular), Cu (dioptase), Na

(albite), K (sanidine); *M_β* lines: U (metallic U). Other elements, including S, Si or Mg were also sought, but they were not found (the detection limits of the analysis for these elements are ~0.1 wt. % with the analytical conditions used). Peak counting times were 10–20 s and the counting time for the background was 50 % of those on the peak. The measured intensities were converted to elemental concentrations using the *PAP* program (Pouchou and Pichoir 1985).

The results of electron microprobe analyses are summarized in Tab. 2. The empirical formula of linekrite (based on 30.22 O *apfu*) is (K_{1.73}Na_{0.02})_{Σ1.75}(Ca_{2.97}Cu_{0.02})_{Σ2.99}

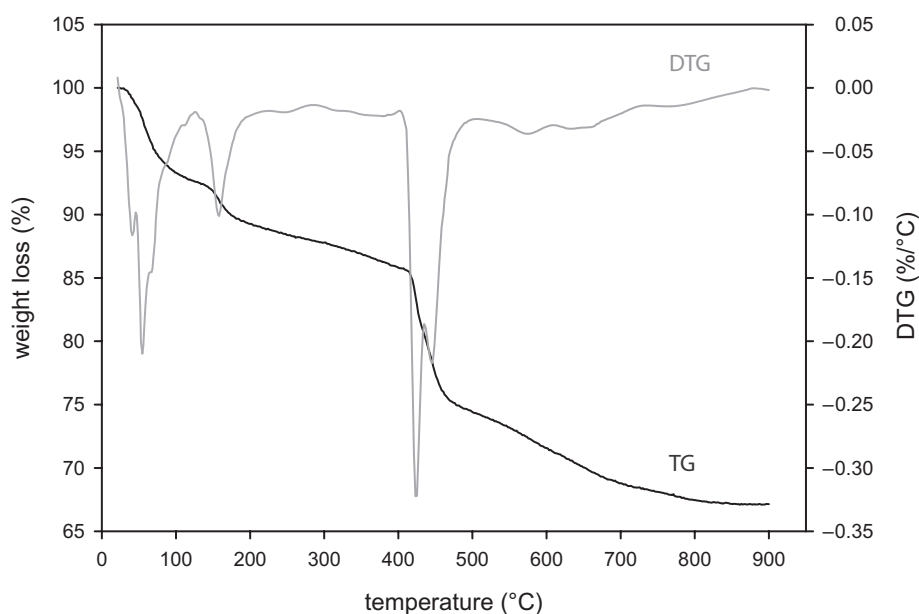


Fig. 3 Thermal gravimetry curves for linekrite.

Tab. 1 Thermal analysis of línekite

Temperature	Weight loss (wt. %)	Mass units	Assignment
125	7.392	91.875	5 H ₂ O (exp. 5.10 H ₂ O)
188	3.113	38.691	2 H ₂ O (2.15 H ₂ O)
413	3.941	48.983	1 H ₂ O + 1 CO ₂ (0.76 H ₂ O + 0.8 CO ₂)*
483	10.738	133.463	3 CO ₂ (3.03 CO ₂)
900	7.675	95.393	2 CO ₂ (2.17 CO ₂)
total	32.858	408.405	8 H ₂ O + 6 CO ₂ (8.01 H ₂ O + 6 CO ₂)

* data assigned tentatively

[(UO₂)(CO₃)₃]_{2.02}(H₂O)₈. The basis of 30.22 O in the calculation was chosen due to charge balance. The ideal formula of línekite is K₂Ca₃[(UO₂)(CO₃)₃]₂8H₂O, which requires K₂O 7.58, CaO 13.54, CO₂ 21.25, UO₃ 46.03, H₂O 11.60, total 100.00 wt. %. The Gladstone–Dale compatibility index 1–(K_v/K_c) is –0.001 for the empirical formula, indicating a superior compatibility (Mandarino 1981).

6. Raman and infrared spectroscopy

The Raman spectrum (Fig. 4) of línekite was collected using a DXR dispersive Raman spectrometer (Thermo Scientific) mounted on a confocal Olympus microscope (100× objective). The Raman signal was excited by a 532 nm diode-pumped solid-state laser and then detected by a CCD detector. Experimental parameters: exposure time, 10 s; number of exposures, 32; grating, 400 lines/mm; spectrograph aperture, 50 μm slit; camera temperature, –50 °C; laser power level, 3.0 mW. The instrument was calibrated by a software-controlled calibration procedure using multiple neon emission lines (wavelength calibration), multiple polystyrene Raman bands (laser frequency calibration) and standardized white light sources (intensity calibration). For acquiring the infrared spectrum of línekite (Fig. 5), a micro diffuse reflectance infrared Fourier transform spectroscopy (micro-DRIFTS) was utilized. The Thermo Nicolet 6700 FTIR spectrometer (range 4000–600 cm^{–1}, resolution 4 cm^{–1}, 128 scans, Happ–Genzel apodization) equipped with a Spectra Tech InspectIR Plus micro-spectroscopic accessory (mercury–

Tab. 2 Chemical composition of línekite

Constituent	Mean of 28 points (wt. %)	Range	Stand. Dev.
Na ₂ O	0.06	0.00–0.28	0.07
K ₂ O	6.89	6.53–7.34	0.21
CaO	14.11	13.28–14.78	0.35
CuO	0.12	0.00–0.53	0.18
CO ₂ *	22.51		
UO ₃	48.76	47.63–50.04	0.59
H ₂ O*	12.20		
Total	104.65		

Contents of H₂O and CO₂* were calculated from stoichiometry derived from the thermal analysis

cadmium–telluride detector) was employed. A small amount of the sample was pulverized and mixed with a portion of KBr and immediately analyzed without preparation the pellet. The same KBr without the specimen was taken as the blank reference. Spectra were processed (background correction, fitting)

using OMNIC Spectral tool software v.7.3 (Thermo Fisher Scientific Inc.). The Raman and infrared spectra of línekite are interpreted with regard to the papers by Koglin et al. (1979), Anderson et al. (1980), and Čejka (1999, 2005).

6.1. O–H vibrations

The Raman and infrared bands and shoulders in the region above 2500 cm^{–1} (Raman bands at 3500, 3470, 3270, 3080, 2900 and 2740 cm^{–1} and infrared bands and shoulders at 3590, 3500, 3380, 3220, 3010, 2730 and 2570 cm^{–1}) were assigned to ν O–H stretching frequencies of structurally non-equivalent (symmetrically distinct) H₂O molecules bonded in the structure by the network of H-bonds. According to the empirical relation provided by Libowitzky (1999), the O···O separation distances of the hydrogen bonds vary approximately between 2.9 and 2.6 Å (based on Raman) or between 3.2 and 2.6 Å (based on infrared). A band observed in the Raman spectrum at 1667 cm^{–1} and infrared bands and shoulders at 1698, 1654 and 1609 cm^{–1} are attributed to the ν₂ (δ) bending vibrations of symmetrically distinct H₂O molecules. The weak infrared bands at 788 and at 623 cm^{–1} may be connected with libration modes of H₂O.

6.2. CO₃^{2–} vibrations

Raman bands and shoulders at 1590, 1564, 1392 and 1346 cm^{–1} and infrared bands at 1580, 1553, 1522, 1389 and 1364 cm^{–1} are attributed to the ν₃ antisymmetric stretching vibrations of structurally nonequivalent CO₃ planar groups. The observed splitting of the ν₃ bands indicates the presence of bidentately bonded carbonate groups onto uranyl hexagonal bipyramids in the crystal structure.

Raman bands and shoulders at 1095, 1085 and 1070 cm^{–1} and infrared band at 1069 cm^{–1} were assigned to the ν₁ symmetric stretching vibration of the CO₃ groups. The Raman band at 836 cm^{–1} and infrared bands at 853 and 833 cm^{–1} are attributed to the ν₂ (δ) out-of-plane bending vibration of CO₃. Some overlap of the ν₂ (δ) CO₃ bending vibration with the ν₁ UO₂²⁺ symmetric stretching vibration can be expected. Raman bands and shoulders

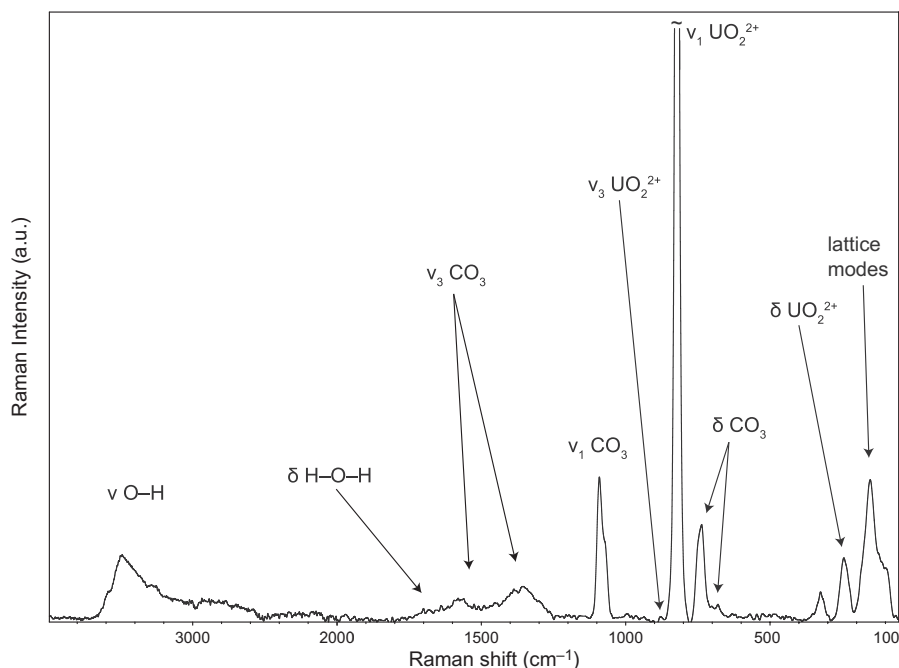


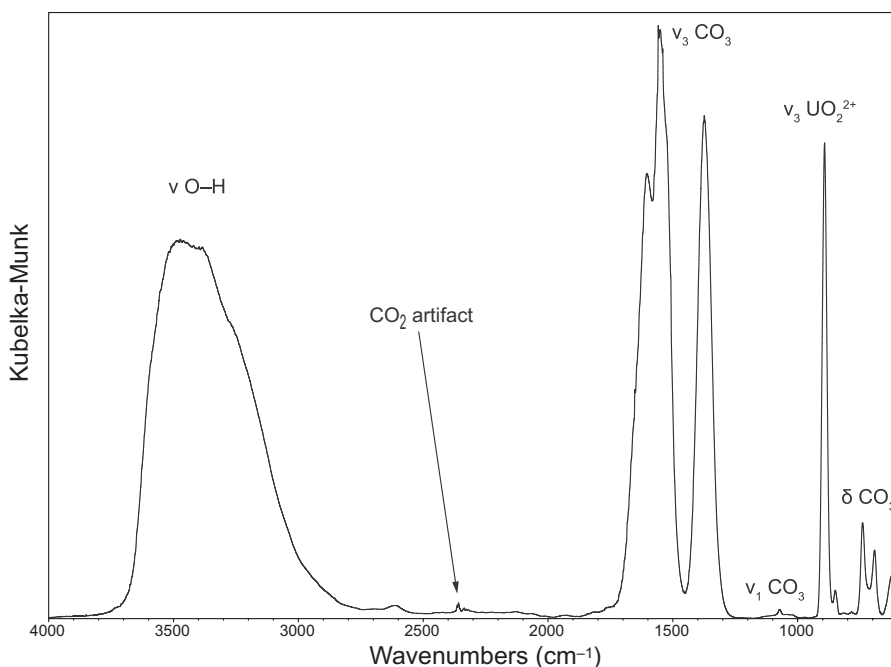
Fig. 4 Raman spectrum of línekite.

at 750, 735, 704 and 680 cm^{-1} and infrared bands at 752, 738, 694 and 658 cm^{-1} are assigned to the ν_4 (δ) in-plane bending CO_3 vibration.

6.3. Vibrations of UO_2^{2+}

The Raman band at 822 cm^{-1} and infrared band at 809 cm^{-1} belong to the ν_1 symmetric stretching mode of UO_2^{2+} and an infrared band at 892 cm^{-1} to the ν_3 antisymmetric stretching mode of UO_2^{2+} . As noted above, some overlap with the ν_2 of CO_3 cannot be excluded. According to the relation provided by Bartlett and Cooney (1989), U–O bond lengths inferred from the wavenumbers of uranyl stretching vibrations vary in the range of 1.78–1.80 Å. Those values are in agreement with the values given by Burns et al. (1997) for uranyl ions coordinated in hexagonal bipyramids. The Raman bands at 339, 324 and 298 cm^{-1} may be related to the ν ($\text{U}-\text{O}_{\text{ligand}}$) stretching vibrations and those bands at 249 and 236 cm^{-1} are connected with the ν_2 (δ) bends of uranyl. However, some overlaps may be expected in this spectral region. Bands at the lowest wavenumbers were assigned to lattice modes.

Fig. 5 The infrared spectrum of línekite.



7. X-ray crystallography and crystal structure

Powder x-ray diffraction data of línekite were collected from a capillary sample in Debye-Scherrer geometry using a PANalytical Empyrean powder diffractometer equipped with a Cu X-ray tube (45 kV, 40 mA), PIXcel3D solid-state detector and primary focusing Göbel mirror optics. The powder pattern was measured from 3 to 80° 2θ with a step size 0.013° 2θ and a counting time 1 s per step. The repeated scan option was utilized

Tab. 3 Powder X-ray diffraction data (d_{hkl} in Å) for línekite

I_{rel}	Línekite (this paper)						Meyrowitz et al. (1964)	
	d_{obs}	d_{calc}	I_{calc}	h	k	l	d_{obs}	I_{rel}
1	10.306	10.316	2	1	1	1		
1	9.186	9.183	3	0	0	2		
100	8.627	8.627	100	2	0	0	8.70	100
60	6.436	6.435	84	0	2	2	6.40	36
4	6.231	6.234	7	2	2	0	6.25	4
9	6.028	6.029	3	1	2	2	6.03	7
11	5.935	5.937	21	2	1	2	5.95	13
2	5.712	5.715	2	0	3	1	5.73	4
8	5.492	5.495	16	1	1	3	5.50	11
3	5.422	5.425	9	1	3	1	5.43	4
43	5.153	5.158	98	2	2	2	5.17	46
5	4.932	4.933	11	2	3	0	4.94	6
1	4.858	4.860	2	1	2	3		
1	4.710	4.689	<1	3	2	1		
19	4.592	4.591	30	0	0	4	4.60	31
12	4.505	4.510	23	0	4	0	4.51	11
8	4.360	4.346	2	2	3	2	4.37	11
6	4.311	4.313	5	4	0	0	4.32	20
5	4.195	4.195	5	4	1	0	4.21	14
3	4.153	4.163	<1	1	3	3	4.17	4
5	4.083	4.083	4	3	1	3		
15	4.053	4.053	22	2	0	4	4.06	24
10	3.996	3.997	20	2	4	0	4.00	11
5	3.953	3.954	8	2	1	4		
4	3.903	3.904	4	4	0	2		
5	3.813	3.816	8	4	1	2		
3	3.786	3.801	5	3	2	3		
2	3.703	3.697	2	2	2	4		
11	3.583	3.583	27	4	2	2		
4	3.549	3.549	2	3	4	0		
4	3.525	3.523	6	1	1	5		
7	3.504	3.505	16	4	3	0		
4	3.480	3.484	3	3	4	1		
1	3.392	3.391	2	5	0	1		
2	3.339	3.338	1	1	2	5		
4	3.275	3.274	5	4	3	2		
4	3.218	3.217	9	0	4	4		
1	3.163	3.163	1	1	4	4		
3	3.144	3.144	6	4	0	4		
3	3.118	3.117	12	4	4	0		
8	3.097	3.097	9	4	1	4		
4	3.061	3.061	3	0	0	6		
2	3.044	3.051	2	3	1	5		
4	3.015	3.015	9	2	4	4		
1	2.992	2.993	<1	5	3	0		
2	2.963	2.962	1	1	6	0		
1	2.955	2.952	1	4	4	2		
1	2.926	2.924	1	1	6	1		
5	2.900	2.899	10	0	2	6		
1	2.877	2.885	1	2	0	6		
5	2.862	2.857	10	0	6	2		
7	2.853	2.852	7	5	2	3		
5	2.843	2.849	4	2	1	6		
8	2.820	2.819	3	1	6	2		

d values quoted in Å

to improve the counting statistics with an accumulation of 40 scans. Before the measurement, the diffractometer was calibrated against a LaB₆ capillary standard. Positions of the diffraction peaks were refined using the pseudo-Voigt profile function using least-squares of the High-Score Plus program (PANalytical). The unit cell parameters were refined from the powder data by Celref program (Laugier and Bochu 2014) using the diffraction peaks up to 45°2θ (99 diffractions). The hkl indices were taken from the calculated powder diffraction pattern obtained from the PowderCell program (Kraus and Nolze 1996). The refined unit-cell parameters of línekite are: $a = 17.254(4)$ Å, $b = 18.040(4)$ Å, $c = 18.366(4)$ Å and $V = 5717(2)$ Å³. The powder data for línekite are listed in Tab. 3.

A 0.31 × 0.25 × 0.11 mm large green crystal of línekite was selected for the single-crystal X-ray diffraction experiment using an Oxford diffraction Gemini single-crystal diffractometer, with monochromated MoK_α radiation ($\lambda = 0.71073$ Å; 55 kV, 38 mA) from a sealed X-ray tube monochromatized with a graphite monochromator, collimated with a fiber-optics Mo-Enhance collimator, and detected with an Atlas CCD detector. The best crystal selected for the diffraction experiment was, however, found to be a split crystal with partially overlapping reflections. A twin-matrix for determining the overlaps of partially and fully separated reflections was later used in the refinement of the structure. The crystallographic details with the parameters for the data collection and refinement are listed in Tab. 4. The intensity data were corrected

for Lorentz factor, polarization and background. The absorption correction, combining numerical shape-based correction and the empirical scaling, was done in Jana2006 software (Petříček et al. 2014), leading to the $R_{\text{int}} = 0.046$.

The structure of línekitite was solved independently from the known structure of the synthetic phase (Hughes-Kubatko and Burns 2004). The refinement of that model in Jana2006 software (Petříček et al. 2014), using our dataset, led only to the less-satisfactory results, corresponding to higher residuals: the R ($[I_{\text{obs}} > 3\sigma(I)] = 0.049$ and wR ($[I_{\text{obs}} > 3\sigma(I)] = 0.119$ with $\text{GOF} = 2.15$; maximal and minimal peaks in the difference-Fourier electron-density were 4.93 and $-2.53 \text{ e } \text{Å}^{-3}$. Therefore a new structure solution was carried out using SIR2002 software (Burla et al. 2003) in the space group $Pnmm$, which was chosen based on the reflection conditions. The model obtained was subsequently refined in Jana2006 using a full-matrix least-squares algorithm based on F^2 employed therein. The refinement confirmed that the structure of línekitite is extremely pseudosymmetric and contains a high degree of disorder, involving especially disordered C, O sites (of the H_2O molecules), and K sites, with considerably lowered occupations of the corresponding sites. That disorder corresponds to larger differences between línekitite structure and the structure of the synthetic phase, which is also responsible for the less accuracy of the

refinement while using the structure of synthetics as a starting model for the least-squares refinement. The final cycle of the refinement converged with the residuals R ($[I_{\text{obs}} > 3\sigma(I)] = 0.0340$ and wR ($[I_{\text{obs}} > 3\sigma(I)] = 0.0783$ with $\text{GOF} = 1.82$; maximal and minimal peaks in the difference-Fourier electron-density were 3.00 and -1.12

Tab. 3 Continued

I_{rel}	d_{obs}	Línekitite (this paper)					Meyrowitz et al. (1964)	
		d_{calc}	I_{calc}	h	k	l	d_{obs}	I_{rel}
3	2.812	2.810	2	1	4	5		
1	2.803	2.808	1	3	4	4		
4	2.786	2.786	3	4	3	4		
9	2.749	2.748	12	2	2	6		
4	2.745	2.744	3	6	0	2		
1	2.729	2.734	3	3	5	3		
4	2.712	2.712	11	2	6	2		
2	2.691	2.689	3	5	3	3		
1	2.652	2.650	4	4	5	2		
2	2.580	2.579	12	4	4	4		
3	2.560	2.559	2	3	6	2		
2	2.554	2.552	1	3	4	5		
<1	2.545	2.546	<1	1	5	5		
1	2.525	2.525	3	1	7	1		
4	2.498	2.496	3	6	3	2		
1	2.491	2.493	2	1	2	7		
1	2.469	2.471	2	5	5	1		
1	2.422	2.423	<1	5	2	5		
2	2.416	2.415	2	6	1	4		
3	2.407	2.406	5	4	2	6		
2	2.382	2.382	5	4	6	2		
4	2.369	2.366	7	3	1	7		
3	2.347	2.344	2	6	4	2		
2	2.309	2.308	4	3	2	7		
1	2.296	2.296	2	0	0	8		
2	2.220	2.218	2	2	0	8		
1	2.213	2.212	5	4	7	0		
2	2.198	2.197	4	5	4	5		
1	2.185	2.184	1	4	4	6		
2	2.150	2.151	2	4	7	2		
1	2.143	2.144	1	6	4	4		
1	2.124	2.126	2	5	6	3		
3	2.108	2.106	5	1	5	7		
5	2.094	2.094	3	1	7	5		
3	2.083	2.082	2	6	1	6		
1	2.077	2.078	2	6	6	0		
2	2.065	2.065	1	5	7	0		
2	2.061	2.063	1	5	5	5		
4	2.035	2.035	7	5	2	7		
3	2.029	2.030	1	8	3	0		
2	2.023	2.024	2	0	8	4		
2	2.012	2.014	1	1	1	9		
2	1.9933	1.9930	2	4	7	4		
3	1.9899	1.9907	5	3	5	7		
1	1.9788	1.9794	1	1	9	1		

d values quoted in Å

$\text{e } \text{Å}^{-3}$. Refined atom coordinates, displacement parameters, and occupation factors are given in Tab. 5. The bond-valence analysis of the structure was carried out following the procedure of Brown (1981, 2002), based on the refined interatomic distances (Electronic Supplementary Material 1), and is provided in the Electronic

Tab. 4 Data collection and structure refinement for línekite

Crystal data	
Formula	$K_{1.952}Ca_3[(UO_2)(CO_3)_3]_2(H_2O)_{7.164}$
Crystal system	orthorhombic
Space group	<i>Pnnm</i>
Unit-cell parameters: <i>a</i> , <i>b</i> , <i>c</i> [Å]	17.0069(5), 18.0273(5), 18.3374(5)
Unit-cell volume [Å ³]	5622.0(3)
Z	8
Calculated density [g/cm ³]	2.904 (for the above given formula)
Crystal size [mm]	0.31 × 0.25 × 0.11
Data collection	
Diffractometer	Oxford Diffraction Gemini with Atlas detector
Temperature [K]	300
Radiation, wavelength [Å]	MoK _α , 0.71073 (50 kV, 30 mA)
θ range for data collection [°]	2.7728.40
Limiting Miller indices	<i>h</i> = −15→21, <i>k</i> = −23→20, <i>l</i> = −23 → 23
Axis, frame width (°), time per frame (s)	ω, 1.0, 100
Total reflections collected	34219
Unique reflections	6179
Unique observed reflections, criterion	4468, [<i>I</i> > 3σ(<i>I</i>)]
Absorption coefficient [mm ^{−1}], type	12.942, multi-scan
T_{min}/T_{max}	0.097/0.344
R_{int}	0.046
F_{000}	4405
Structure refinement by Jana2006	
No. of ref. param., restraints, constraints	429, 0, 6
<i>R</i> , <i>wR</i> (obs)	0.0339, 0.0782
<i>R</i> , <i>wR</i> (all)	0.0545, 0.0839
GOF obs/all	1.82, 1.64
Weighting scheme, weights	σ, $w = 1/(\sigma^2(I) + 0.0004I^2)$
Largest diff. peak and hole (e [−] /Å ³)	−1.26, 3.61
Twin fractions	0.93(1), 0.07(1)
Twin matrix	$\begin{pmatrix} 1 & -0.02 & -0.04 \\ 0.03 & 1 & 0 \\ 0.05 & 0 & 1 \end{pmatrix}$

Supplementary Material 2. Moreover, the CIF file, also containing a block with the reflections, is deposited at the Journal's web page www.jgeosci.org.

7.1. Crystal structure

There are three U⁶⁺ sites, nine C⁴⁺ sites (including two split-sites; positionally disordered from their corresponding special positions at the mirror planes), four Ca²⁺ sites, six K⁺ sites and thirty-seven O sites (including split-sites), eleven of which are occupied by the molecular H₂O.

The three independent U⁶⁺ sites are each coordinated by two, strongly bonded O atoms at the distance of ~1.8 Å (Electronic Supplementary Material 1), forming uranyl ions, UO₂²⁺. These are in turn further coordinated by six O atoms, arranged at the equatorial vertices of hexagonal bipyramids. Each bipyramid is chelated by three CO₃ groups

attached bidentately to the bipyramid to form the uranyl tricarbonate cluster, [(UO₂)(CO₃)₃]^{4−}. There are four disordered (split) CO₃ groups, C5 and C5', C7 and C7', linked to the U2 and U3 hexagonal bipyramids. The uranyl tricarbonate clusters are not attached directly to each other, but through the Ca–O bonds they are connected into sheets stacked perpendicular to **a**.

The four sites, occupied by Ca²⁺, are coordinated in a distinct way in the línekite structure (Fig. 6). The Ca1 site is coordinated by seven ligands including one H₂O group (O26w) linked to the four U⁶⁺ sites. The Ca2 site is also linked to the four U⁶⁺ sites (symmetrically related U1 sites, U2 and U3), coordinated by seven ligands, including one H₂O group (O27w), linking the K5 site. The Ca3 site is located at the mirror plane and is coordinated by the six ligands (three of them are split sites), linked to the four U⁶⁺ sites (symmetrically related U1 sites, U2 and U3). Among the ligands linked to the Ca3 site we can observe increased disorder manifested in large thermal parameters for the O24/O24', O27w/O27w', and O31w/O31w' atoms, modeled in the current refinement as the split sites. Finally, the Ca4 site is linked only to a single U site (U3) via symmetrically related O22 atom and further coordinated by seven ligands, including positionally disordered H₂O

molecules (O31w and O31w', modeled as split-sites). All Ca²⁺ sites were found to be fully occupied. Linkage of the uranyl tricarbonate clusters and Ca²⁺ polyhedra results in the sheets, stacked along (100), which are the most rigid part of the línekite structure. The basic unit of these compact regions in the structure is a cluster we refer to as paddle-wheel structure, where two Ca²⁺ (Ca1 and Ca2) are linked via four CO₃ groups of four distinct [(UO₂)(CO₃)₃]^{4−} clusters (Fig. 6). In línekite, each uranyl tricarbonate cluster is a part of two paddle-wheels (Fig. 7) that link them into a square-grid (Fig. 8a), composed of the orthorhombic-distorted tetragonal Ca₂(H₂O)₂[(UO₂)(CO₃)₃]₂ layers, leading to strongly pseudo-tetragonal diffraction pattern (Fig. 8b). The paddle-wheel motif is characteristic of related uranyl carbonate minerals and compounds (Vochten et al. 1994; Mereiter 1986b; Hughes-Kubatko and Burns 2004; Mereiter 2013).

Tab. 5 Atom site occupancies, coordinates and displacement parameters ($U_{\text{iso}}/U_{\text{eq}}$ in \AA^2) for línkite

Occ.	x/a	y/b	z/c	$U_{\text{iso}}/U_{\text{eq}}$	U^{11}	U^{22}	U^{33}	U^{12}	U^{13}	U^{23}
U1	0.207596(15)	0.239027(14)	0.225854(15)	0.02236(9)	0.02471(15)	0.01780(13)	0.02457(17)	0.00021(10)	0.00438(10)	-0.00057(12)
U2	0.76697(2)	0.48990(2)	0	0.02423(14)	0.0306(2)	0.0246(2)	0.0176(2)	0.00595(15)	0	0
U3	0.76647(2)	0.02820(2)	0	0.02529(14)	0.0291(2)	0.0290(2)	0.0178(2)	-0.00855(16)	0	0
Ca1	0.32298(8)	0.42930(8)	0.18733(8)	0.0210(5)	0.0246(8)	0.0192(7)	0.0192(9)	0.0013(5)	0.0010(6)	-0.0003(6)
Ca2	0.32491(8)	0.04955(8)	0.18639(8)	0.0206(5)	0.0260(8)	0.0175(7)	0.0182(8)	-0.0004(5)	0.0012(6)	0.0004(6)
Ca3	0.46676(13)	0.24034(11)	0	0.0267(7)	0.0358(13)	0.0223(10)	0.0220(12)	-0.0003(9)	0	0
Ca4	0.06448(14)	-0.18296(12)	0	0.0328(8)	0.0336(14)	0.0309(12)	0.0338(14)	-0.0067(9)	0	0
K1	-0.02733(18)	0.2292(2)	0.21506(17)	0.0667(14)	0.050(2)	0.103(3)	0.046(2)	-0.0096(17)	-0.0039(13)	-0.0151(17)
K2	0	0.5	0	0.073(3)	0.043(4)	0.117(6)	0.059(5)	-0.002(3)	0	0
K3	0.5437(7)	0.4529(8)	-0.0601(6)	0.148(7)	0.143(12)	0.175(12)	0.126(11)	-0.123(9)	-0.056(7)	0.059(8)
K4	0.2198(4)	0.2742(4)	0	0.049(3)	0.050(5)	0.060(5)	0.037(5)	-0.001(3)	0	0
K5	0.5378(6)	0.0291(6)	0.0395(6)	0.067(4)	0.054(8)	0.060(7)	0.087(8)	0.021(4)	0.025(5)	0.011(5)
K6	0.7138(9)	0.2547(9)	0	0.118(10)	0.076(13)	0.092(13)	0.19(2)	-0.009(8)	0	0
C1	0.1386(5)	0.1000(4)	0.2634(4)	0.028(3)	0.031(5)	0.019(4)	0.035(5)	0.001(3)	0.003(3)	0.003(4)
C2	0.3587(4)	0.2398(4)	0.1546(4)	0.025(2)	0.029(4)	0.025(4)	0.022(4)	0.003(3)	0.003(3)	0.002(3)
C3	0.3621(4)	-0.1229(4)	0.2333(5)	0.029(3)	0.023(4)	0.025(4)	0.039(5)	0.000(3)	0.004(3)	0.003(4)
C4	0.3322(5)	0.0553(4)	0.3637(4)	0.029(3)	0.035(5)	0.030(4)	0.021(5)	-0.008(3)	0.002(3)	0.005(4)
C5	0.3476(14)	0.3956(14)	0	0.022(3)*						
C5'	0.3680(14)	0.4072(13)	0	0.022(3)*	0.027(4)	0.027(4)	0.019(5)	-0.003(3)	0.001(3)	0.002(3)
C6	0.1719(4)	-0.0832(4)	0.1360(4)	0.024(2)						
C7	0.3597(14)	0.0773(12)	0	0.027(4)*						
C7'	0.3291(13)	0.1053(13)	0	0.027(4)*						
O1	0.1595(3)	0.2374(3)	0.1396(3)	0.039(2)	0.044(4)	0.039(3)	0.033(3)	-0.005(3)	-0.004(3)	-0.001(3)
O2	0.2555(3)	0.2404(3)	0.3115(3)	0.038(2)	0.041(3)	0.039(3)	0.033(4)	0.001(3)	0.002(3)	0.002(3)
O3	0.2982(3)	-0.1261(3)	0.2702(3)	0.0301(18)	0.028(3)	0.022(3)	0.040(4)	0.001(2)	0.013(2)	-0.002(3)
O4	0.397(3)	-0.1861(3)	0.2237(3)	0.0355(19)	0.033(3)	0.020(3)	0.054(4)	0.000(2)	0.015(3)	0.009(3)
O5	0.1038(3)	0.1621(3)	0.2721(3)	0.040(2)	0.036(3)	0.020(3)	0.063(4)	0.005(2)	0.020(3)	0.008(3)
O6	0.3193(3)	0.2998(3)	0.1677(3)	0.037(2)	0.042(3)	0.017(3)	0.053(4)	-0.001(2)	0.025(3)	-0.001(3)
O7	0.2063(3)	0.1037(3)	0.2313(3)	0.0309(18)	0.031(3)	0.020(3)	0.042(4)	-0.001(2)	0.014(3)	0.001(2)
O8	0.3225(3)	0.1799(3)	0.1733(3)	0.038(2)	0.037(3)	0.017(3)	0.060(4)	0.003(2)	0.025(3)	0.004(3)
O9	0.6991(5)	0.4139(4)	0	0.040(3)	0.037(5)	0.026(4)	0.055(6)	-0.003(3)	0	0
O10	0.8348(5)	0.5663(4)	0	0.038(3)	0.040(5)	0.039(5)	0.036(5)	-0.001(4)	0	0
O11	0.3289(3)	0.4308(3)	0.0590(3)	0.038(2)	0.056(4)	0.045(4)	0.014(3)	0.024(3)	0.004(3)	0.000(3)
O12	0.3581(3)	0.0794(3)	0.4269(3)	0.036(2)	0.039(4)	0.047(3)	0.020(3)	-0.022(3)	0.000(2)	-0.002(3)
O13	0.2733(3)	0.0121(3)	0.3663(3)	0.0332(19)	0.042(4)	0.038(3)	0.019(3)	-0.015(2)	-0.003(2)	0.001(3)
O14	0.6911(5)	0.0963(5)	0	0.042(3)	0.041(5)	0.047(5)	0.037(5)	0.004(4)	0	0
O15	0.8415(5)	-0.0421(4)	0	0.043(3)	0.043(6)	0.034(5)	0.053(6)	-0.001(4)	0	0
O16	0.1505(3)	-0.1079(3)	0.0715(3)	0.0320(19)	0.043(4)	0.037(3)	0.016(3)	-0.015(2)	-0.002(2)	-0.002(2)
O17	0.3216(4)	0.0579(4)	0.0591(3)	0.052(2)	0.064(5)	0.072(5)	0.020(3)	-0.045(4)	-0.003(3)	0.003(3)
O18	0.2280(3)	-0.0343(3)	0.1329(3)	0.0323(19)	0.036(4)	0.037(3)	0.023(3)	-0.016(2)	-0.001(2)	-0.004(3)
O19	0.1097(3)	0.0402(3)	0.2864(3)	0.036(2)	0.030(3)	0.025(3)	0.053(4)	-0.003(2)	0.008(3)	0.012(3)

Tab. 5 Continued

Occ.	x/a	y/b	z/c	$U_{\text{iso}}/U_{\text{eq}}$	U^{11}	U^{22}	U^{33}	U^{12}	U^{13}	U^{23}
O20	0.1389(3)	-0.1032(3)	0.1931(3)	0.0344(19)	0.041(4)	0.045(3)	0.018(3)	-0.009(3)	0.005(2)	0.005(3)
O21	0.3901(3)	-0.0637(3)	0.2082(3)	0.037(2)	0.030(3)	0.021(3)	0.060(4)	0.000(2)	0.015(3)	0.007(3)
O22	0.3658(3)	0.0747(3)	0.3062(3)	0.040(2)	0.049(4)	0.053(4)	0.01(3)	-0.014(3)	0.002(3)	-0.004(3)
O23	0.4266(3)	0.2398(3)	0.1285(3)	0.0289(17)	0.027(3)	0.029(3)	0.030(3)	0.001(2)	0.009(2)	0.001(2)
O24	0.4228(10)	0.3654(9)	0	0.035(3)*						
O24*	0.3862(10)	0.3392(9)	0	0.035(3)*						
O25	0.4168(9)	0.1213(8)	0	0.035(3)*						
O26	0.3493(9)	0.1683(8)	0	0.035(3)*						
O27w	0.5771(10)	0.2651(9)	0.0765(9)	0.073(3)*						
O27w'	0.5787(9)	0.2060(10)	0.0771(8)	0.073(3)*						
O28w	0.1215(4)	-0.2695(3)	0.0850(4)	0.055(3)	0.072(5)	0.039(4)	0.056(5)	-0.003(3)	-0.024(4)	0.006(3)
O29w	-0.0239(5)	-0.1373(6)	0.0919(5)	0.105(4)	0.075(6)	0.124(8)	0.114(8)	-0.022(5)	0.027(5)	-0.066(7)
O30w	-0.0375(6)	-0.2799(6)	0	0.077(5)	0.069(8)	0.077(7)	0.085(8)	-0.036(6)	0	0
O31w	0.0306(7)	0.3891(7)	0.1207(7)	0.100(4)*						
O31w'	0.008(3)	0.478(2)	0.1552(19)	0.100(4)*						
O32w	0.006(2)	0.067(2)	0.035(2)	0.06(2)*						
O33w	0.5	0.5	0.3351(5)	0.053(4)	0.037(6)	0.066(6)	0.057(7)	-0.013(4)	0	0
O34w	0.4598(3)	0.3989(4)	-0.1643(3)	0.048(2)	0.031(4)	0.070(4)	0.044(4)	0.010(3)	0.005(3)	0.015(3)
O35w	0.4609(3)	0.0825(3)	0.1588(3)	0.040(2)	0.027(3)	0.042(3)	0.050(4)	-0.003(2)	0.000(3)	0.015(3)

* – split site; w – H₂O site; * – refined with isotropic atomic displacement parameters

There are six sites in the structure of línekite, occupied by K⁺ cations. All sites have reduced occupancies, as documented from the site-scattering, varying from ~85% to ~25% site-occupancy. Hydrated potassium cations represent the least firm part of the structure. The refinement K and O atoms (of the H₂O groups) is particularly difficult due to driven pseudosymmetry of just slightly orthorhombic-distorted tetragonal Ca₂(H₂O)₂[(UO₂)(CO₃)₃]₂ layers. The assignment of whether the site is dominantly occupied by H₂O and/or K⁺, is conclusively not straightforward in the case of línekite. Here in case of such pseudosymmetry, the fact that K–O bond lengths are similar to the O··O distances for the hydrogen-bonded H₂O molecules makes the entire issue difficult. The current approach resulting in the presented structure model is based on the fact that disordered K or Ca atoms still tend to provide sharper Fourier peaks than the disordered H₂O molecules. The effect of pseudosymmetry in línekite can be demonstrated on the K2 site and its coordination environment in particular. The K2 sitting on a mirror plane is coordinated by fourteen ligands, among them, eight are symmetrically related split atom sites (O32w, O32w'). We can also view it as that the K2 coordination polyhedra are squeezed between two paddle-wheel structures, which can induce such disorder in coordinated, partly occupied H₂O sites. The final content of K⁺ per unit cell obtained from the site-scattering refinement is 1.952 atoms, which is nearly the ideal stoichiometric content.

The eleven O sites in línekite structure, including split-sites, belong to the molecular H₂O, according to the bond-valence analysis (Electronic Supplementary Material 2) and the coordination scheme. Except for O34w atom, located in the cavity of the framework, all other O sites occupied by H₂O molecules are coordinated to Ca²⁺ and namely to K⁺ cations. The majority of H₂O molecules in the structure are positionally disordered and have also a considerably lowered occupation. The phenomenon mentioned above is driven again by the strong pseudosymmetry of Ca₂(H₂O)₂[(UO₂)(CO₃)₃]₂ layers where no desymmetrization takes place. The only ordered and fully occupied H₂O sites are coordinated to Ca²⁺ cations within the layers. The refinement of the O site occupancies, associated with the H₂O sites, yielded the sum of 7.164 H₂O per the unit cell.

8. Discussion – relationship to the synthetic analogs and other uranyl carbonates, the stoichiometry and the water content of línekite

Línekite, the synthetic phase prepared by Meyrowitz et al. (1964) and the synthetics by Hughes-Kubatko and Burns (2004) are essentially isostructural. The synthetic

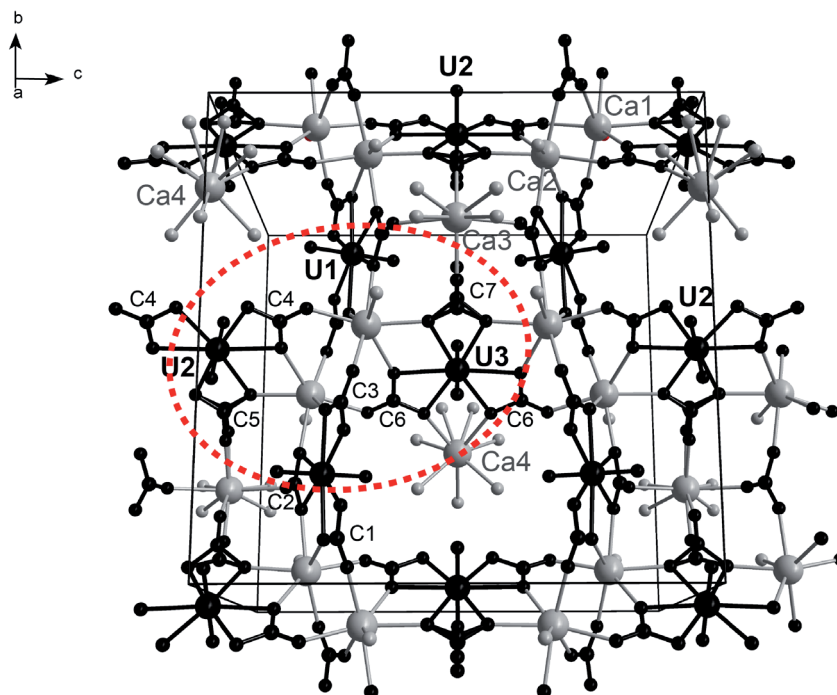


Fig. 6 The (100) sheet of the nominal composition $\{\text{Ca}_3[(\text{UO}_2)_2(\text{CO}_3)_3]\}_2^{2-}$ in the structure of línekite. The red dashed eclipse marks the “paddle-wheel” motif. Each uranyl tricarbonate cluster is involved in the two “paddle-wheels”.

phase prepared by Meyrowitz et al. (1964) has a unit-cell of the dimensions $a = 17.98$, $b = 18.29$, $c = 16.95$ Å; space groups inferred $Pn\bar{m}n$ or $Pn2n$. The powder data provided by Meyrowitz et al. (1964) fit very well to the diffraction data of línekite (Tab. 2) and the indices of refraction are also in the range, $\alpha = 1.544(3)$, $\beta = 1.549(3)$, $\gamma = 1.5'63(3)$.

The cationic content in the formula of línekite obtained from the structure refinement, $\text{K}_{1.952}\text{Ca}_3[(\text{UO}_2)(\text{CO}_3)_3]_2(\text{H}_2\text{O})_{7.165}$ ($Z = 8$), is close to the ideal stoichiometry $\text{K}:\text{Ca} = 2:3$. The results of electron microprobe analysis, however, gave a lower K^+ content, $(\text{K}_{1.73}\text{Na}_{0.02})_{\Sigma 1.75}(\text{Ca}_{2.97}\text{Cu}_{0.02})_{\Sigma 2.99}$. This not unreasonable, due to the overlap of K K_α and U K_α peaks in the spectrum and consequent problems while measuring exact concentrations of K , even in the WDS mode. We are convinced that the cationic content in línekite is similar to the other related uranyl

tricararbonates containing alkali- or earth-alkaline cations (Mereiter 1986a, b, 2013), showing no departures from the ideal stoichiometry. It is possible that a small amount of excessing Ca^{2+} cations could also entry the K sites in the structure; however, this is not the case. The only known non-stoichiometric exception among uranyl tricararbonates is a synthetic phase of Vochten et al. (1994),

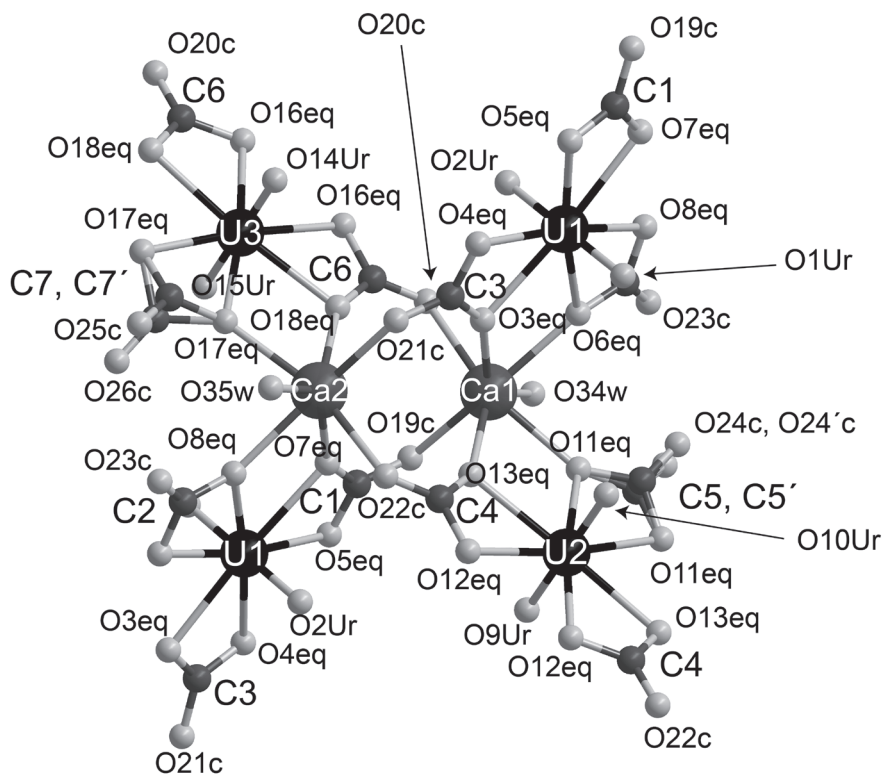


Fig. 7 The “paddle-wheel” in línekite structure, where the two Ca^{2+} cations take part in linkage to four uranyl tricarbonate clusters. The $\text{Ca1}-\text{Ca2}$ distance is 4.05 Å. Captions to abbreviations: Ur – apical O atom of the UO_2^{2+} ion; eq – equatorial O atom of the UO_8 ; OXc – O atom no. X of the CO_3 group; w – H_2O site; ' – split site.

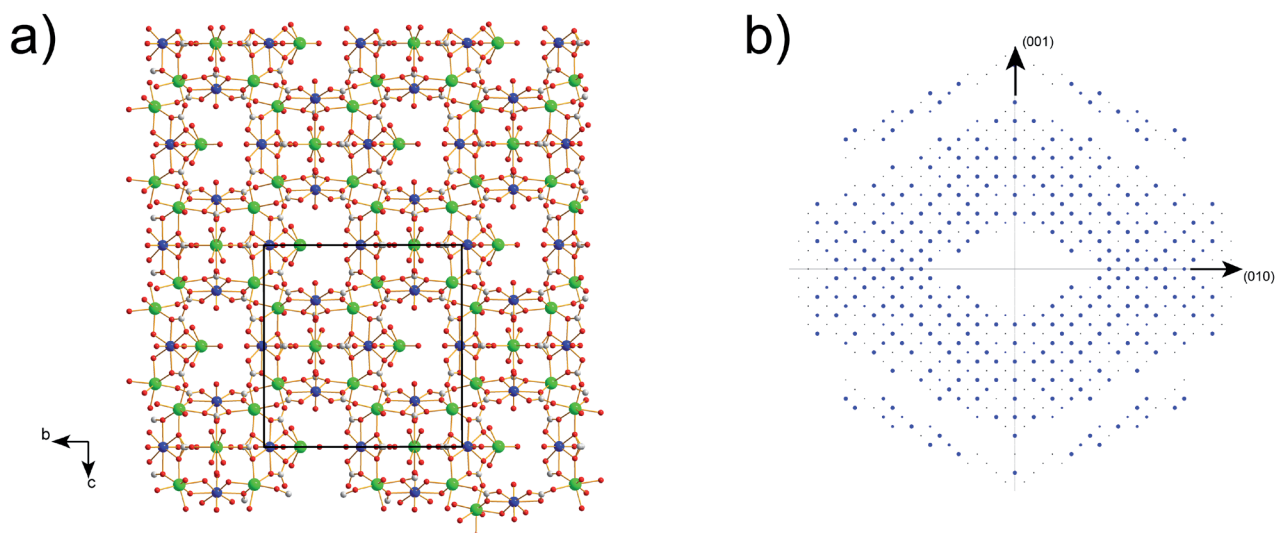


Fig. 8 The square grid of the (100) sheet in the structure of línekite (a) leading to the strongly pseudo-tetragonal diffraction pattern (b). The latter was calculated by Jana2006 as F_{calc} for the contributions of the U and Ca atoms only.

$\text{Ca}_{1.54}\text{Na}_{0.63}[(\text{UO}_2)(\text{CO}_3)_3](\text{H}_2\text{O})_{\sim 5.38}$. This compound, noteworthy, has a similar unit-cell metrics as línekite ($a = 18.2$, $b = 16.9$, $c = 18.4$ Å, $Z = 8$, space group: $Pnmm$). Línekite has an extremely pseudosymmetric structure and a high degree of disorder; consequently, the structure refinement is problematic. The content of molecular H_2O both in línekite and in the synthetic analog by Hughes-Kubatko and Burns (2004), obtained from the refinement of single-crystal X-ray data only, is thus underestimated. The only reliable values can be obtained from the chemical analysis (thermogravimetric or gas/vapor-absorption measurement in a combustion train) in the case of such a high-degree disorder as present in the structure of línekite (since no desymmetrization takes place there).

Acknowledgements. The authors thank Ladislav Lapčák (Institute of Chemical Technology, Prague) for the collection of the Raman spectrum of línekite and Karla Fejfarová (BIOCEV, Prague) for help with X-ray data collection. Kurt Mereiter (TU Vienna) is highly acknowledged for the discussion on the línekite, a thorough critical reading of the manuscript and reviews on the earlier versions of the text. Comments by František Veselovský and an anonymous referee as well as handling editor František Laufek helped in improving the manuscript. This research was financially supported the project No. LO1603 under the Ministry of Education, Youth and Sports National sustainability program I of Czech Republic to JP, MD and by the long-term project DKRVO 2017-01 of the Ministry of Culture of the Czech Republic (National Museum 000232782) to JS and JČ.

Electronic supplementary material. Supplementary crystallographic data for this paper (including the selected

interatomic distances, results of bond-valence analysis and a CIF file) are available online at the Journal website (<http://dx.doi.org/10.3190/jgeosci.241>).

References

- ANDERSON A, CHIEH CH, IRISH DE, TONG, JPK (1980) An X-ray crystallographic, Raman, and infrared spectral study of crystalline potassium uranyl carbonate, $\text{K}_4\text{UO}_2(\text{CO}_3)_3$. *Canad J Chem* 58: 1651–1658
- BARTLETT JR, COONEY RP (1989) On the determination of uranium–oxygen bond lengths in dioxouranium(VI) compounds by Raman spectroscopy. *J Mol Struct* 193: 295–300
- BRESE NE, O'KEEFFE M (1991) Bond-valence parameters for solids. *Acta Cryst B* 47: 192–197
- BROWN ID (1981) The bond-valence method: an empirical approach to chemical structure and bonding. In: O'KEEFFE M, NAVROTSKY A (eds) *Structure and Bonding in Crystals*, Vol. 2. Academic Press, New York, pp 1–30
- BROWN ID (2002) *The Chemical Bond in Inorganic Chemistry: The Bond Valence Model*. Oxford University Press, Oxford, pp 1–230
- BROWN ID, ALTERMATT D (1985) Bond-valence parameters obtained from a systematic analysis of the inorganic crystal structure database. *Acta Cryst B* 41: 244–247, with updated parameters from http://www.ccp14.ac.uk/ccp/web-mirrors/i_d_brown/
- BURLA MC, CAMALLI M, CARROZZINI B, CASCARANO GL, GIACOVAZZO C, POLIDORI G, SPAGNA R (2003) SIR2002: the program. *J Appl Cryst* 36: 1103
- BURNS PC, EWING RC, HAWTHORNE FC (1997) The crystal chemistry of hexavalent uranium: polyhedron geometries, bond-valence parameters, and polymerization of polyhedra. *Canad Mineral* 35: 1551–1570

- ČEJKA J (1969) To the chemistry of andersonite and thermal decomposition of dioxo-tricarbonatouranates. *Coll Czechoslov Chem Commun* 34: 1635–1656
- ČEJKA J (1999) Infrared spectroscopy and thermal analysis of the uranyl minerals. In: BURNS PC, FINCH RC (eds) *Uranium: Mineralogy, Geochemistry and the Environment*. Mineralogical Society of America and Geochemical Society Reviews in Mineralogy and Geochemistry 38: pp 521–622
- ČEJKA J (2005) Vibrational spectroscopy of the uranyl minerals – Infrared and Raman spectra of the uranyl minerals II. Uranyl carbonates. *Bull mineral-petrolog Odd Nár Muz (Praha)* 13: 62–72 (in Czech)
- HUGHES-KUBATKO KA, BURNS PC (2004) The crystal structure of a novel uranyl tricarbonate, $K_2Ca_3[(UO_2)(CO_3)_3]_2(H_2O)_6$. *Canad Mineral* 42: 997–1003
- KOGLIN E, SCHENK HJ, SCHWOCHAU K (1979) Vibrational and low temperature optical spectra of the uranyl tricarbonate complex $[UO_2(CO_3)_3]^{4-}$. *Spectrochim Acta A35*: 641–647
- KRAUS W, NOLZE G (1996) POWDER CELL – a program for the representation and manipulation of crystal structures and calculation of the resulting X-ray powder patterns. *J Appl Cryst* 29: 301–303
- KRIVOVICHEV SV, PLÁŠIL J (2013) Mineralogy and crystallography of uranium. In: BURNS PC, SIGMON GE (eds) *Uranium: From Cradle to Grave*. Mineralogical Association of Canada Short Courses 43: pp 15–119
- LANGMUIR D (1978) Uranium solution–mineral equilibria at low temperatures with applications to sedimentary ore deposits. *Geochim Cosmochim Acta* 42: 547–569
- LAUGIER J, BOCHU B (2014) CELREF: unit cell refinement program from powder diffraction diagram. *Laboratoires des Matériaux et du Génie Physique, Ecole Nationale Supérieure de Physique de Grenoble (INPG), Grenoble, France*. Accessed on May 30, 2014, at <http://www.ccp14.ac.uk/tutorial/lmgp/celref.htm>
- LIBOWITZKY E (1999) Correlation of O–H stretching frequencies and O–H···O hydrogen bond lengths in minerals. *Monatsh Chem* 130: 1047–1059
- MANDARINO JA (1981) The Gladstone–Dale relationship: Part IV. The compatibility concept and its application. *Canad Mineral* 19: 441–450
- MEREITER K (1984) The crystal structure of albrechtschraufite, $MgCa_4F_2[(UO_2)(CO_3)_3]_2 \cdot 17H_2O$. *Acta Crystallogr A40 Supplement*: C–247
- MEREITER K (1986a) Crystal structure and crystallographic properties of schröckingerite from Joachimsthal. *Tschermaks Mineral Petrogr Mitt* 35: 1–18
- MEREITER K (1986b) Neue Kristallographische Daten über das Uranmineral Andersonit. *Anzeig Österr Akad Wiss Matem-Naturwiss Kl* 1986/3: 39–41
- MEREITER K (2013) Description and crystal structure of albrechtschraufite, $MgCa_4F_2[UO_2(CO_3)_3]_2 \cdot 17-18H_2O$. *Mineral Petrol* 107: 179–188
- MEYROWITZ R, ROSS DR, ROSS M (1964) A new uranyl tricarbonate, $K_2Ca_3(UO_2)_2(CO_3)_6 \cdot 9-10H_2O$. *US Geol Surv, Prof Pap* 501B: 82–83
- ONDROUŠ P, SKÁLA R, VESELOVSKÝ F, SEJKORA J, VITTI C (2003) Čejkaite, the triclinic polymorph of $Na_4(UO_2)(CO_3)_3$ – a new mineral from Jáchymov, Czech Republic. *Amer Miner* 88: 686–693
- PETŘÍČEK V, DUŠEK M, PALATINUS L (2014) Crystallographic computing system Jana 2006: general features. *Z Kristallogr* 229: 345–352
- PLÁŠIL J, FEJFAROVÁ K, DUŠEK M, ŠKODA R, ROHLÍČEK J (2013) Revision of the symmetry and crystal structure of čejkaite, $Na_4(UO_2)(CO_3)_3$. *Amer Miner* 98: 549–553
- PLÁŠIL J, HLOUŠEK J, KASATKIN AV, BELAKOVSKIY DI, ČEJKA J, CHERNYSHOV D (2015) Ježekite, $Na_8[(UO_2)(CO_3)_3](SO_4)_2 \cdot 3H_2O$, a new uranyl mineral from Jáchymov, Czech Republic. *J Geosci* 60: 259–267
- PLÁŠIL J, MEREITER K, KAMPF A R, HLOUŠEK J, ŠKODA R, ČEJKA J, NĚMEC I, EDEROVÁ J (2016) Braunerite, IMA2015-123. *CNMNC Newsletter No. 31, June 2016*, page 692; *Mineral Mag* 80: 691–697
- POUCHOU JL, PICOIR F (1985) “PAP” (φρΖ) procedure for improved quantitative microanalysis. In: ARMSTRONG JT (ed) *Microbeam Analysis*. San Francisco Press, San Francisco, pp 104–106
- SCHRAUF A (1873) Schröckingerit, ein neues Mineral von Joachimsthal. *Tschermaks Mineral Petrogr Mitt* 3: 137–138
- SKÁLA R, ONDRUŠ P, VESELOVSKÝ F, CÍSAŘOVÁ I, HLOUŠEK J (2011) Agricolaite, a new mineral of uranium from Jáchymov, Czech Republic. *Mineral Petrol* 103: 169–175
- VOCHTEN R, VAN HARVERBEKE L, VAN SPRINGEL K, BLATON N, PEETERS OM (1994) The structure and physicochemical characteristics of a synthetic phase compositionally intermediate between liebigite and andersonite. *Canad Mineral* 32: 553–561